

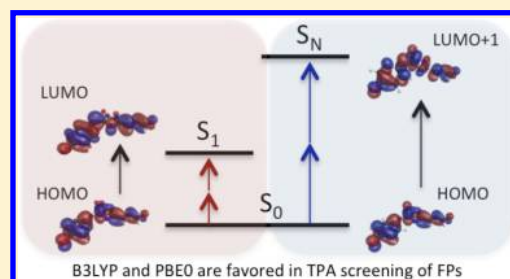
Two-Photon Absorption in Fluorescent Protein Chromophores: TDDFT and CC2 Results

M. Alaraby Salem and Alex Brown*

Department of Chemistry, University of Alberta, Edmonton, Alberta T6G 2G2 Canada

S Supporting Information

ABSTRACT: Two-photon spectroscopy of fluorescent proteins is a powerful bioimaging tool. Considerable effort has been made to measure absolute two-photon absorption (TPA) for the available fluorescent proteins. Being a technically involved procedure, there is significant variation in the published experimental measurements even for the same protein. In this work, we present a time-dependent density functional theory (TDDFT) study on isolated chromophores comparing the ability of four functionals (PBE0, B3LYP, CAM-B3LYP, and LC-BLYP) combined with the 6-31+G(d,p) basis set to reproduce averaged experimental TPA energies and cross sections. The TDDFT energies and TPA cross sections are also compared to corresponding CC2/6-31+G(d,p) results for excitation to S_1 for the five smallest chromophores. In general, the computed TPA energies are less functional dependent than the TPA cross sections. The variation between functionals is more pronounced when higher-energy transitions are studied. Changes to the conformation of a chromophore are shown to change the TPA cross-section considerably. This adds to the difficulty of comparing an isolated chromophore to the one embedded in the protein environment. All functionals considered give moderate agreement with the corresponding CC2 results; in general, the TPA cross sections determined by TDDFT are 1.5–10 times smaller than the corresponding CC2 values for excitation to S_1 . LC-BLYP and CAM-B3LYP give erroneously large TPA cross sections in the higher-energy regions. On the other hand, B3LYP and PBE0 yield values that are of the same order of magnitude and in some cases very close to the averaged experimental data. Thus, based on the results reported here, B3LYP and PBE0 are the preferred functionals for screening chromophores for TPA. However, at best, TDDFT can be used to semiquantitatively scan chromophores for potential TPA probes and highlight spectroscopic peaks that could be present in the mature protein.



1. INTRODUCTION

Fluorescent proteins generally refer to the fluorescent homologues of the green fluorescent protein (GFP) of *Aequorea victoria*. After the discovery of GFP in the 1960s,¹ and later the cloning of the gene,² it has been shown that GFP can be expressed in other organisms and yet remain fluorescent.^{3,4} Significant investment has been made into improving the photophysical properties of fluorescent proteins (FP) for their nonobtrusive use in real-time bioimaging. A great variety of fluorescent proteins have been synthesized and characterized, spanning a broad spectrum from blue to red fluorescent proteins.^{5,6} The color of fluorescence is mainly controlled by the chromophore that is formed by three precursory residues.^{7,8} By altering these amino acids, different maturation routes lead to different chromophore structures (many examples are mentioned in this work). In addition to the chromophore, the surrounding protein structure can also influence various photophysical properties of the protein.⁶ The close-by residues to the chromophore can profoundly change the color of fluorescence, as seen in some variants of GFP that are shifted to produce yellow instead of green light albeit having the same chromophore as in GFP.⁹

Two-photon spectroscopy of cells expressing FPs has received less attention than one-photon spectroscopy but is

recently gaining more interest.⁵ It is less damaging to the biological system, as it involves the absorption of photons of longer wavelengths (and lower energy). Furthermore, the two-photon absorption (TPA) probability is proportional to the square of the incident light intensity. This provides better focus and less out-of-focus photobleaching, which makes two-photon microscopy preferred for imaging thick tissues with deeper penetration and reduced autofluorescence. Since one-photon absorption (OPA) and TPA follow different quantum-mechanical selection rules, they can be used in a complementary fashion.

In most of the studied FPs, excitation at nearly twice the one-photon wavelength peak results in effective TPA followed by fluorescence. The TPA peak is generally blue-shifted.^{10,11} Recent computational studies on the chromophore of GFP showed that this blue-shift is mainly due to the vibronic coupling of states related to the bridge between the chromophore rings causing a non-Condon effect.^{12,13} A detailed model of the shift has been developed and applied to a family of red FPs.¹⁴ List et al. have carried out a detailed computational study at the CAM-B3LYP/6-31+G(d) level of

Received: January 14, 2014

theory for the isolated DsRed chromophore and the FP in order to ascertain the role of the protein environment on TPA.¹⁵ Another interesting feature in the TPA profile of FPs is the presence of additional peak(s) in the shorter wavelength (higher energy) region where there is no corresponding significant one-photon absorption (OPA). This was first predicted by time-dependent density functional theory (TDDFT) computations¹⁶ and then experiments showed very strong TPA in this region.¹⁷ Theoretical investigations reveal that excitations to higher excited states of the chromophores yield these bands. These transitions have been shown to be enhanced due to near-resonance conditions,^{16,18} as further confirmed in this study. An early application for this high-energy band has been introduced using the red fluorescent protein, DsRed.¹⁹ A newer technique was presented employing the simultaneous stimulation of blue and red FPs at the wavelength corresponding to the low-energy absorption and high-energy absorption of each, respectively.²⁰

Measuring the probability of TPA (i.e., the TPA cross-section) is technically demanding. Several parameters that need experimental evaluation produce experimental errors that contribute to the uncertainty of the absolute cross-section. Recently, a thorough measurement of TPA for many of the available FPs was conducted within a wide spectral range.¹⁷ The data shows that the bands that overlap between OPA and TPA profiles do not necessarily show equivalent intensities. The spectral window of these measurements could show the strong TPA in the high-energy regions, but it was not enough to fully resolve the spectral peaks in many cases; that is, truncating the spectra before reaching the energy corresponding to the maximal TPA cross-section.

Theoretical studies of the TPA properties of fluorescent proteins are likewise challenging. A combined quantum mechanics/molecular mechanics approach was used in a recent study to reproduce the OPA and TPA of GFP.²¹ The computation succeeded in reproducing most of the experimental structural features of the TPA spectrum, but failed in obtaining the absolute TPA cross sections. Other studies focused on isolated models of the chromophores.^{16,20} Although the TPA of a chromophore can be largely influenced by the protein environment, studying the isolated chromophore was shown to be a useful starting point to understand the photophysical properties of the FP.¹⁶ The study we present here evaluates the use of four different functionals to compute the TPA of seven FP chromophores in the TDDFT framework. We compare TPA cross sections computed for different models at various computational levels to experimental data, to CC2 results, and to previous computational work. Several related studies on other systems have been conducted previously.^{22–26} In a pioneering computational study of TPA, Paterson et al.²² demonstrated that CAM-B3LYP provides the best agreement with benchmark CC3 results; interestingly, the same study shows B3LYP values appear superior when comparing with the TPA cross sections determined using more computationally accessible CC2 methods. A study to evaluate TDDFT methods for determining the TPA of oligophenylvinyls discouraged the use of the long-range corrected functional (LC-BLYP) and favored B3LYP.²³ It also suggested the exclusion of diffuse functions from the basis sets. Another study on donor- π -acceptor molecules favored PBE0 to B3LYP for stilbene-based and fluorene-based compounds.²⁴ Our findings concerning the functional performance are generally in accordance with these previous studies. A recent study of the effect of the π - π

stacking on the TPA of the YFP utilized RICC2 and TDDFT with the CAM-B3LYP functional.²⁵ The results show very good qualitative agreement between both methods, which led to the conclusion that TDDFT is suitable for examining the TPA of the charge-transfer transitions in YFP. However, scaling had to be employed to match the shifted energies and cross sections. A benchmark of TDDFT against RICC2 favored the use of CAM-B3LYP over other functionals, including B3LYP, for computing the TPA of aromatic compounds with strong charge-transfer character in many of the low-lying electronic states.²⁶ This may lead to the preference for CAM-B3LYP to B3LYP, since non-long-range corrected functionals are known to have problems with charge-transfer states. In the present work, we further explore which functional, if any, is the best choice for efficient screening of TPA for FP chromophores in the framework of TDDFT, which is based on response theory.

2. COMPUTATIONAL METHODS

2.1. Chromophore Structures. The investigated chromophores are shown in Figure 1. The chromophore structures

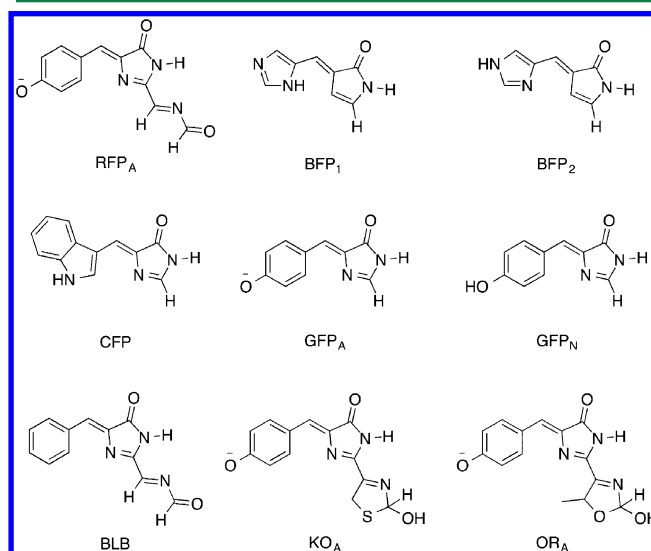


Figure 1. Models for chromophores named after common fluorescent proteins they represent.

were obtained by breaking the connections to the protein backbone and capping with hydrogen atoms. In these models, the π -conjugated system important for TPA is preserved. The chromophores were chosen to represent proteins for which TPA cross sections have been consistently measured by Drobizhev et al.¹⁷ to avoid the variability observed in the experimental measurements of a given FP. RFP represents the chromophore of red fluorescent proteins²⁷ such as DsRed.²⁸ Here, we include a carbonyl from the adjacent amino acid to account for the extra acylimine substituent that results from an additional dehydrogenation step during the RFP maturation.²⁹ This acylimine moiety is also included in BLB that represents the chromophore of mBlueberry1³⁰ and similar proteins. The blue fluorescent protein BFP^{31,32} is represented by two models, BFP₁ and BFP₂, to account for its two possible protonation states. CFP represents the chromophore of ECFP³² and similar proteins where Tyr 66 is replaced by Trp.³² Two models were used in the case of the green fluorescent protein (GFP)⁸ to represent the possible protonation states of the chromophore,

as both states are fluorescent in its wild-type.³³ KO_A and OR_A represent mKo³⁴ and mOrange^{35,36} proteins, respectively.

2.2. Theory and Computations. Geometries of the reported model chromophores were optimized in the gas phase using the hybrid Perdew, Burke, and Ernzerhof exchange-correlation density functional PBE0^{37,38} and the 6-31+G(d,p) basis set.^{39–43} Coordinates for the optimized structures can be found in Table S1 and Table S2 in the Supporting Information. Excitation energies, OPA oscillator strengths (OS), and TPA cross sections were computed with time-dependent density functional theory⁴⁴ (TDDFT) employing linear⁴⁵ and quadratic response theory.^{46–48} Several functionals have been investigated for determining the photophysical properties: B3LYP,⁴⁹ PBE0, the long-range corrected B3LYP adopting the Coulomb-attenuating method (CAM-B3LYP),⁵⁰ and the long-range corrected version of the correlation functional of Becke, Lee, Yang, and Parr (LC-BLYP)^{51–54} in both the gas phase and using the conductor-like polarizable continuum model (C-PCM, and herein referred to simply as PCM)^{55–58} with parameters for water. Transition dipole moments between excited states were determined in the gas phase only, as the computation was very sensitive to cavitation parameters when PCM was used for solvation. The TPA for the smallest chromophores with Cs symmetry (BFP₁, BFP₂, GFP_A, GFP_N, and CFP) were also computed using the second order approximate coupled clusters singles and doubles model, CC2.^{59,60} In all DFT, TDDFT, and CC2 computations, the 6-31+G(d,p) basis set using Cartesian harmonics was employed, except where noted. For one-photon absorption, the oscillator strength (i.e., the transition probability) of a transition from the ground state $|0\rangle$ to an excited state $|f\rangle$ is given by

$$\delta^{\text{OPA}} = \frac{2\omega_f}{3} \sum_{\alpha} |\langle 0|\mu_{\alpha}|f\rangle|^2 \quad (1)$$

where ω_f is the excitation energy from ground state to state f and μ_{α} is the dipole moment operator for a certain Cartesian coordinate α . For two-photon absorption, the two-photon transition matrix has elements

$$S_{\alpha\beta} = \sum_n \left[\frac{\langle 0|\mu_{\alpha}|n\rangle\langle n|\mu_{\beta}|f\rangle}{\omega_n - \frac{\omega_f}{2}} + \frac{\langle 0|\mu_{\beta}|n\rangle\langle n|\mu_{\alpha}|f\rangle}{\omega_n - \frac{\omega_f}{2}} \right] \quad (2)$$

where n ranges from the ground state 0 to the final excited state f . Assuming that the polarization of incident light is linear, the transition moment for TPA is

$$\delta^{\text{TPA}} = \sum_{\alpha\beta} [S_{\alpha\alpha}S_{\beta\beta}^* + 2S_{\alpha\beta}S_{\alpha\beta}^*] \quad (3)$$

The two-photon absorption cross-section, which can be related to the experimental measurements, is then

$$\sigma^{\text{TPA}} = \frac{4\pi^2 a_0^5 \alpha \omega_f^2}{15c \Gamma} \delta^{\text{TPA}} \quad (4)$$

where a_0 is the Bohr radius, α is the fine structure constant, c is the speed of light, and Γ is the lifetime broadening which is assumed to be 0.1 eV for comparison to experiment as employed before.⁶¹ All factors should be inserted in eq 4 in atomic units (au) and the result is converted from au to GM units.

To investigate for the presence of charge-transfer states, the overlap quantity Λ is reported.⁶² It is a nonunique diagnostic value that measures the degree of overlap between virtual and occupied orbitals for a given excitation. The Λ values range from 0 to 1 where small values indicate the evidence for long-range excitations (Rydberg-type or charge-transfer).

CC2 computations, the computations of permanent dipole moments of excited states, and transition dipole moments between excited states were done using the DALTON⁶³ software package. All other computations were carried out with GAMESS⁶⁴ (May-2012 version), and all computations with C-PCM have utilized default parameters. MacMolPlt,⁶⁵ version 7.5, was used to generate plots of the primary orbitals involved in the excitations.

3. RESULTS AND DISCUSSION

Comparing computed TPA cross sections to experimental measurements is a very challenging task. One reason is the great variation between experimental measurements of TPA cross sections for the same fluorescent protein.¹⁷ For instance, reported cross sections for one peak of EGFP⁶⁶ vary from 1.5 GM⁶⁷ to 180 GM.⁶⁸ To relate our results to a consistent experimental reference, we limit our comparison to the results published by Drobizhev et al.¹⁷ Another problem is that each chromophore is found in different proteins and the protein environment affects its photophysical behavior especially in the case of TPA cross-section.¹⁴ TPA depends on the difference between permanent dipole moments of a given excited state and the ground state in addition to its dependence on transition dipole moments, as can be seen in the sum-of-states expression (eq 2). Therefore, the electric field within the protein can strongly affect the TPA absorption.¹⁷ In addition, changes in the chromophore conformation itself due to the surrounding protein residues strongly affect the TPA absorption, as discussed in section 3.1. Hence, we choose to compare our computed values to the average values of cross sections for the proteins that share the same chromophore when a range of values is available. The conclusions drawn from such comparison will only be qualitative or semiquantitative in nature, but the knowledge of maximum and minimum values of the data range included in an average shed light on possible effects of local environment (including electric field) and conformation on the TPA cross-section. We also compare (some of) the TDDFT results to those determined using the significantly more computationally demanding CC2 method. In the following sections, we first discuss the lowest-energy transition to S_1 (section 3.1) and then the higher energy transitions to S_n (section 3.2), where n is the excited state of interest, which varies according to the system (i.e., chromophore) and the computational method. These should correspond to the band of the longest wavelength and other band(s) of shorter wavelengths in the experimental TPA spectrum of a given protein, respectively. For each chromophore, we computed 8 excitations per functional for TDDFT; for CC2, only S_1 is reported, as higher states were difficult to converge for many of the systems. In section 3.2, we first provide a thorough analysis of the data determined for the higher transitions for one chromophore, namely RFP. Further, we only report data for the most significant transitions and compare these to the available experimental data. Full data of the 8 excitations as determined using TDDFT, including excitation energies, Λ values, OPA oscillator strengths, and

Table 1. Excitation Energies and TPA Cross Sections for the Transitions to S_1 (Bands of Lower Energy and Longer Wavelengths) as Determined at the TDDFT/6-31+G(d,p) Level of Theory in PCM (H_2O) and at the CC2/6-31+G(d) Level of Theory in the Gas Phase^a

model	energy (eV)							TPA cross-section (GM)						
	B3LYP	PBE0	CAM	LC	CC2	expt.	prev. calc.	B3LYP	PBE0	CAM	LC	CC2	expt.	prev. calc. ^b
RFP _A	2.28	2.31	2.32	2.29	2.26	2.26 (2.18–2.36)	2.36	4	5	9	13		56 (15–139)	22.7
BFP ₁	3.40	3.46	3.55	3.59	3.78	3.31	3.59	3	3	7	11	45	12	1.32
BFP ₂	3.59	3.66	3.79	3.83	4.09	3.31	3.62	4	5	8	10	10	12	0.00
CFP	3.14	3.23	3.37	3.41	3.58	2.85	3.32	30	28	28	31	102	23	24.74
GFP _A	2.96	3.00	3.02	2.97	2.89	2.83 (2.68–2.87)	2.97	4	4	9	15	10	46 (12–85)	0.59
GFP _N	3.34	3.41	3.56	3.62	3.80	3.11 (3.06–3.21)	3.46	17	17	21	25	80	36 (15–56)	5.58
KO _A	2.45	2.50	2.59	2.58		2.38		27	27	31	30		41	
OR _A	2.48	2.53	2.6	2.59		2.30	2.59	22	22	25	25		67	12.87
BLB	2.68	2.77	3.04	3.19	3.24	3.05		90	94	101	93		4	

^aExperimental values are averages for the values measured by Drobizhev et al.¹⁷ in the cases where the model is represented by several proteins (range is given when applicable) and previous calculations refer to those by Nifosi and Luo.¹⁶ Experimental energies are doubled to match the OPA energies computed by the different methods. ^bReported to the same number of decimal places as given by Nifosi and Luo.¹⁶ Details of level of theory provided in main text.

TPA cross sections, for all chromophores is provided in the Supporting Information (Tables S3, S4, and S5).

3.1. LOWEST-ENERGY TRANSITION TO S_1

The one-photon energies and TPA cross sections from this work and previous computational work by Nifosi and Luo¹⁶ are shown in Table 1 together with the corresponding experimental measurements. In Table 1, the experimental data correspond to average values for the excitation energies and TPA cross sections of different proteins sharing the same chromophore. Throughout this paper, experimental energies are multiplied by a factor of 2 for ease of comparison to the computational data - no correction is made for the blue-shift observed in the TPA of many FPs.^{13,14} The experimental data for specific proteins considered are grouped by chromophore in Table S6 in the Supporting Information. To obtain the average, proteins with colors significantly shifted from other proteins sharing the same chromophore were excluded: from the proteins sharing the GFP chromophore, the yellow homologues were omitted and from the proteins sharing the RFP_A chromophore, we excluded tagBFP⁶⁹ that is blue-shifted. mKok, mOrange, and mBlueberry1 were the only proteins of their types in the experimental data set, so KO_A, OR_A and BLB are compared directly to the values for these proteins, respectively.

As shown in Table 1, different functionals under study yield values very close to the energetics for the S_1 transition—similar to what has been shown in previous OPA and TPA studies.^{16,70} Our results indicate that the energetics are weakly functional dependent with CAM-B3LYP and LC-BLYP giving in most cases slightly higher energies than B3LYP and PBE0. Similar to what has been shown before,⁷⁰ comparison to the previous computations also indicate that energetics are not greatly affected by change of medium and basis; for example, the excitation energies using PCM(H_2O) are approximately 0.1 eV smaller than the gas-phase results, see Supporting Information, Table S5. The energies for the B3LYP and PBE0 functionals are closer to the experimental values (with the exception of BLB). We see that the first model for BFP, namely BFP₁, behaves better than BFP₂ in terms of reproducing the experimental energy. The CC2 energies for the neutral models are larger than those from any of the four functionals (even if one accounted for a small gas-phase to PCM shift) and, thus,

overestimate the experimental measurements. The overestimation for CC2 may be due to the use of the modest 6-31+G(d,p) basis; the size of the systems precluded using a larger basis and, in fact, CC2 results were not obtained for the two largest chromophore models.

Previous calculations by Nifosi and Luo¹⁶ used similar chromophore models but with methyl-group capping (c.f. hydrogen capping in the present study). In the previous study, the B3LYP functional was used in the gas phase employing the following basis sets: 6-31G(d) for all chromophores and 6-31+G(d) for the anionic and some neutral ones. The values reported in Table 1 are for those determined with the diffuse basis functions; that is, 6-31+G(d), except for BFP models. These values deviate 0.19 eV (BFP₁) to 0.01 eV (GFP_A) from the present results at the B3LYP/6-31+G(d,p) in PCM (water) level of theory.

In general, the TPA cross sections are (slightly) more functional dependent, see Table 1. In most cases, CAM-B3LYP and LC-BLYP produce larger TPA cross sections than B3LYP and PBE0. Computations using CAM-B3LYP and LC-BLYP functionals are closer to the experimental measurements of the TPA cross sections with mean absolute error (MAE) of 29 GM and 26 GM, respectively. The difference is not very significant when compared to the MAE for B3LYP and PBE0 (31 GM for both). In general, the TDDFT computed values are lower than the experimental ones except for CFP and BLB. In these two cases, LC-BLYP and CAM-B3LYP still produce higher values than B3LYP and PBE0 suggesting that these long-range corrected functionals simply yield higher values than their standard counterparts. This comparison is further investigated in section 3.2. Comparing the TDDFT results using the B3LYP, PBE0, and CAM-B3LYP functionals in the gas-phase, see Supporting Information, Table S5, to the CC2 values for the five chromophores, one obtains MAEs of 36 GM, 37 GM, and 34 GM, respectively. The CC2 computations were outside the experimental ranges for both energetics and TPA cross sections. Given that CC2 is computationally demanding compared to TDDFT and deviates from the experimental data, we do not encourage implementing CC2 in a screening procedure. It can, however, be used for more in-depth analysis, which is beyond the scope of this work.

Comparison to the previous computational results leads to further insight into the parameters affecting the determination of TPA properties. The RFP chromophore was previously computed at the B3LYP/6-31+G(d) level of theory in the gas phase to have a cross-section of 22.7 GM.¹⁶ Our relevant value using B3LYP/6-31+G(d,p) in PCM (water) is 4 GM. Factors that might affect such change include the different basis set, different medium, different model (methyl vs H-capping), or molecular geometry. In order to investigate these factors, the TPA was determined for different models of the RFP chromophore, see Table 2. Using the same geometry

Table 2. Comparison of Different Computations Performed on the RFP Chromophore Using the B3LYP Functional

medium	basis	capping	carbonyl moiety ^a	cross-section (GM)
PCM	6-31+G(d,p)	H	coplanar	4
gas	6-31+G(d,p)	H	coplanar	6
gas	6-31+G(d)	H	coplanar	6
gas	6-31+G(d)	CH ₃	noncoplanar	34
PCM	6-31+G(d,p)	H	noncoplanar ^b	21

^aThe planar structures with hydrogen-capping and the nonplanar structure with methyl-capping are true minima optimized in the gas phase at the PBE0/6-31+G(d,p) level of theory. ^bSame conformation as the minimized molecule with methyl-capping, but the methyl groups were replaced with hydrogens and the bonds to the hydrogens were adjusted to be of lengths equal to the corresponding bonds in the planar model with hydrogen-capping.

(optimized at the PBE0/6-31+G(d,p) level of theory), we repeated the TPA computation in the gas phase at the B3LYP/6-31+G(d,p) and the B3LYP/6-31+G(d) levels of theory and the results were approximately 6 GM for both. Looking at the available gas phase values in the Supporting Information (see

Tables S3, S4, and S5), one can draw the conclusion that they are generally larger than PCM values. The TPA cross-section of 6 GM is approximately four times smaller than the previously calculated TPA cross-section by Nifosi and Luo.¹⁶ Methyl capping was then tried. The methyl-capped model was optimized at the PBE0/6-31+G(d,p) level of theory in the gas phase and the TPA was computed at the same level of theory as in the previous study (B3LYP/6-31+G(d) in the gas phase). Our result was in accordance with that of the previous work: 34 GM and 22.7 GM, respectively (the difference might be attributed to slightly different geometries and energies). We found that the carbonyl group in the model with methyl capping was not in plane with the molecule when minimized, and this agrees with previous studies that show that the C—N—C=O dihedral angle is off-plane by approximately 30 degrees.^{16,28} Retaining the same geometry that was found by minimizing the structure with methyl-capping, we replaced the methyl groups with H atoms (coordinates are given in Table S2 in the Supporting Information) and recomputed the TPA cross-sections. The result was a significant increase in the TPA cross-section from 4 GM to 21 GM, suggesting the critical role of this out-of-plane carbonyl conformer in the RFP chromophore. Examining the $S_{\alpha\beta}$ elements contributing to the TPA cross-section, see eq 3, the major difference between the nonplanar and planar geometries is an increase in the S_{xx} element. Since the one-photon oscillator strengths for the planar and nonplanar geometries are comparable (i.e., 1.23 and 1.11, respectively), the increase in the TPA cross-section can be attributed to an increase in the permanent dipole moment difference between the excited and ground states (in the x -direction along the long molecular axis) as the FP chromophore goes from the planar to nonplanar geometry. More generally, the results suggest that the chromophore geometry, perhaps

Table 3. Data for Higher Excitations as Computed at the TDDFT/6-31+G(d,p) Level of Theory in PCM (H₂O) for the RFP Chromophore

state ^a	functional experimental ^b	energy (eV)	Λ diagnostic	OPA OS	cross-section (GM)	transition
		3.47 (3.30–3.68)			197 (35–400)	
3	B3LYP	3.32	0.75	0.02	2	H ₋₂ to L
3	PBE0	3.47	0.67	0.02	3	H ₋₂ to L
6	CAM-B3LYP	4.13	0.74	0.09	266	H ₋₁ to L
6	LC-BLYP	4.45	0.72	0.01	1242	H ₋₁ to L
5	B3LYP noncoplanar	3.78	0.57	0.09	63	H ₋₂ to L
6	CAM-B3LYP (gas)	4.18	0.73	0.25	598	H ₋₁ to L
6	B3LYP	3.61	0.41	0.01	12	H ₋₄ to L
6	PBE0	3.76	0.42	0.02	12	H ₋₄ to L
7	CAM-B3LYP	4.27	0.40	0.01	63	H ₋₃ to L
7	LC-BLYP	4.52	0.40	0.01	213	H ₋₄ to L
6	B3LYP noncoplanar	3.84	0.50	0.08	159	H ₋₄ to L
7	CAM-B3LYP (gas)	4.36	0.41	0.01	70	H ₋₄ to L
7	B3LYP	3.83	0.72	0.35	93	H to L ₊₁
7	PBE0	3.91	0.71	0.35	77	H to L ₊₁
4	CAM-B3LYP	3.96	0.73	0.34	92	H to L ₊₁
4	LC-BLYP	4.00	0.71	0.44	1130	H to L ₊₁
3	B3LYP noncoplanar	3.44	0.71	0.12	71	H to L ₊₁
5	CAM-B3LYP (gas)	3.99	0.74	0.11	222	H to L ₊₁

^aStates are given in increasing energy order for the B3LYP functional and grouped with the corresponding PBE0, CAM-B3LYP, and LC-BLYP results according to the nature of excitation. See the discussion in section 3.2. Experimental energies are doubled to match the OPA energies computed by the different methods. ^bThe limits of the range of values contributing to the average are given between brackets.

Table 4. Data for Higher Excitations to S_n for the BFP, CFP, GFP, KO_A , OR_A , and BLB Chromophores as Determined at the TDDFT/6-31+G(d,p) Level of Theory in PCM (H_2O) Solvent and the Corresponding Experimental Measurements^a by Drobizhev et al.¹⁷

state	functional	energy (eV)	Λ diagnostic	OPA OS	cross-section (GM)	transition
BFP ₁	experimental ^b	4.50 (4.49–4.51)			12 (10–16)	
3	B3LYP	4.42	0.69	0.05	47	H ₋₂ to L
3	PBE0	4.54	0.69	0.05	56	H ₋₂ to L
3	CAM-B3LYP	4.88	0.68	0.04	119	H ₋₁ to L
3	LC-BLYP	4.98	0.67	0.05	170	H ₋₂ to L
CFP	experimental	4.51			21 (15–27)	
4	B3LYP	4.07	0.62	0.04	126	H ₋₂ to L
4	PBE0	4.22	0.61	0.02	147	H ₋₂ to L
4	CAM-B3LYP	4.71	0.59	0.00	190	H ₋₂ to L
4	LC-BLYP	4.92	0.56	0.02	78	H ₋₂ to L
GFP _N	experimental	4.43 (4.34–4.51)			31 (27–36)	
4	B3LYP	4.30	0.62	0.02	121	H ₃ to L
4	PBE0	4.44	0.62	0.02	131	H ₃ to L
4	CAM-B3LYP	4.82	0.66	0.02	238	H ₄ to L
4	LC-BLYP	4.93	0.65	0.03	285	H ₄ to L
GFP _A	experimental	4.30 (4.27–4.35)			13 (12–16)	
5	B3LYP	4.23	0.64	0.02	15	H ₋₂ to L
5	PBE0	4.36	0.70	0.01	24	H ₋₂ to L
5	CAM-B3LYP	4.76	0.76	0.01	95	H ₋₂ to L
6	LC-BLYP	4.90	0.73	0.01	188	H ₋₂ to L
KO _A	experimental	3.62			93	
4	B3LYP	3.62	0.67	0.17	77	H to L ₊₁
4	PBE0	3.77	0.67	0.19	107	H to L ₊₁
3	CAM-B3LYP	4.17	0.62	0.32	820	H to L ₊₁
3	LC-BLYP	4.31	0.57	0.31	1355	H to L ₊₁
OR _A	experimental	3.88			200	
3	B3LYP	3.65	0.71	0.11	87	H to L ₊₁
3	PBE0	3.80	0.70	0.13	121	H to L ₊₁
3	CAM-B3LYP	4.21	0.63	0.30	754	H to L ₊₁
3	LC-BLYP	4.35	0.59	0.29	1281	H to L ₊₁
BLB	experimental	4.51			22	
5	B3LYP	3.80	0.60	0.02	233	H ₋₄ to L
5	PBE0	3.96	0.60	0.03	288	H ₋₄ to L
5	CAM-B3LYP	4.48	0.61	0.07	300	H ₋₃ to L
6	LC-BLYP	4.66	0.61	0.08	204	H ₋₃ to L

^aExperimental values for BFP, CFP, and GFP are averages for the experimental values measured by Drobizhev et al.¹⁷ while the values for KO_A , OR_A , and BLB refer to one protein for each. Experimental energies are doubled to match the OPA energies computed by the different methods. ^bThe limits of the range of values contributing to the average are given between brackets when applicable.

influenced by the protein backbone, can strongly impact the TPA as illustrated before.¹⁵

The case of the BLB chromophore is even more interesting. This chromophore is similar to that of RFP, with the exception of the missing hydroxyl group on the benzene ring. The deletion of the OH-group (and adding a hydrogen) induced a huge enhancement in the TPA cross-section of the planar conformer, where the TPA cross-section determined using the B3LYP functional increased from 4 GM to 90 GM; the TPA cross-section increased similarly for the other functionals. To investigate the role of geometry on the photophysical properties, the TPA cross-section for BLB was recomputed after deleting the OH group from the out-of-plane RFP_A model with H-capping (coordinates are given in Table S2 in the Supporting Information). The result was a noticeable decrease in TPA cross-section to 25 GM which is very close to the computed cross-section for the same RFP chromophore model. Therefore, the out-of-plane rotation of the acylimine moiety does not always result in an increase in the TPA. The planar

conformer could be achieved because of the use of hydrogen capping in the model. Of course, this is different from the usual connectivities to the chromophore in the protein that are essentially bulkier and force this out-of-plane rotation. Nevertheless, if it is possible to enforce a planar conformation for BLB through protein engineering, the results suggest the TPA may be strongly enhanced. The large difference between the computed values for the planar, or nonplanar, geometries and the experimentally measured values could be attributed to the strong geometry dependence of the TPA cross-section for BLB. The discrepancy between the experimental value for mBlueberry1 and the computed values (whether the planar or the nonplanar models) is further highlighted in section 3.2 in the discussion of higher excited states for BLB.

3.2. High-Energy Transitions to S_n . The one-photon energies, oscillator strengths, overlap quantity Λ and TPA cross sections for the next lowest energy bright states for the RFP chromophore and all the other chromophores are given in Tables 3 and 4, respectively. The quoted experimental

excitation energies and TPA cross sections represent average values over several proteins containing the same chromophore except in the cases of BLB, KO_A, and OR_A, where only one instance of each FP chromophore is available (see Supporting Information, Table S6). In many cases, the previously reported experimental values for the S_n excitation did not represent a true spectroscopic peak but rather the largest TPA cross-section determined within the experimentally feasible measurement window in each case.¹⁷ The upper-limit for this window (multiplied by a factor of 2) ranges from approximately 4.5 eV for blue fluorescent proteins to approximately 3.5 eV for red fluorescent proteins. The computed data was examined using two criteria: (1) excitations with zero TPA cross sections are not considered; (2) high-energy transitions that are 0.5 eV larger than the experimental upper-limit are excluded from the discussion. Although predicted to have very large cross sections, they might be of limited experimental utility due to the larger energy difference between the emitted photons and the absorbed ones causing the dissipated energy in the non-fluorescent route to be higher. In addition, fluorescent proteins in general would have high TPA cross sections in the range of 532 nm (equivalent to an energy of 4.66 eV, when multiplied by two) because of their tryptophan residues^{71,72}

The remaining excitations are grouped according to visual inspection of the primary orbitals involved in the excitation (see Tables S7–S14 in the Supporting Information). Orbitals are referenced relative to the HOMO (H) and the LUMO (L) using a subscript. Each group of excitations has four transitions (one for each functional) that involve orbitals of similar shapes, but they do not necessarily correspond to the same energy gaps. This is because computations with different functionals did not necessarily yield orbitals in the same order. The groups are ordered according to the relative B3LYP energies and the number of each state is given for reference. All the excitation groups for RFP are given in Table 3 and discussed in detail. For all the other chromophores, only data assumed to be contributing to the corresponding experimental S_n transition is reported in Table 4 and a brief discussion is provided. A full list is available in Tables S15 and S16 in the Supporting Information. The experimental spectra that are referred to in this analysis are found in supplementary Figure 1 of the work of Drobizhev et al.¹⁷

RFP. In Table 3, three of the higher bright excited states are grouped. There is a remarkable variation between functionals concerning the arrangement of orbitals and excited states. The first group of excited states includes the third excitation in the B3LYP and PBE0 computations which corresponds to a transition from H₋₂ to L. As deduced from Supporting Information, Table S7, this transition is mapped to a H₋₁ to L transition in the CAM-B3LYP and LC-BLYP computations which corresponds to the sixth excited state. In this group, B3LYP and PBE0 predict very small cross sections in contrast to CAM-B3LYP and LC-BLYP. The corresponding TPA for the H-capped structure having the off-plane acylimine carbonyl is much larger as computed by B3LYP (63 GM compared to 2 GM for the planar model), showing the dependence of this excitation on the geometry of the model in a way similar to, or even greater than, the S_1 excitation. For the full grouped data for the nonplanar model, see Supporting Information Table S17. The second group of transitions have a small value for the Λ diagnostic indicating a long-range excitation. Such a transition is expected to be characterized better by CAM-B3LYP than B3LYP functionals.⁶² The third group, however,

shows a very strong absorption with all functionals and a relatively large Λ diagnostic indicating a valence-type transition. Examining the data suggests the presence of two peaks of very close energy with the higher energy peak having stronger (or similar) TPA cross-section. This behavior is experimentally noticed in some of the proteins represented by the RFP chromophore. The spectrum of mTangerine,³⁵ for instance, has a small peak at 3.01 eV followed by a stronger rise at 3.57 eV. Another example is seen in the spectrum of tagRFP⁷³ that shows two close peaks around 3.65 and 3.27 eV of comparative strengths. Experimentally, the energy of the second band in the fluorescent proteins having the RFP chromophore averages around 3.47 eV. In all proteins included in this average, this corresponds to the maximum TPA cross-section that was recorded in the high-energy region (according to Drobizhev et al.¹⁷) rather than being a true peak. In addition, this average covers TPA cross-section values ranging from 35 GM to 400 GM. Thus, the quoted experimental data are only good for qualitative, or at best semiquantitative, analysis. Comparing this averaged experimental energy to the third group of transitions where all functionals predict a strong absorption, it is noticeable that B3LYP and PBE0 show more accuracy in predicting the energies than CAM-B3LYP and LC-BLYP—similar to what is noticed in the S_1 analysis. Again, LC-BLYP overestimates the TPA cross-section.

Factors that could contribute to the large cross sections were investigated. Transition dipole moments were computed with CAM-B3LYP as an exemplary functional in the gas phase and the transitions were mapped to the relevant PCM ones (see Table 3) via matching orbital shapes. As reported in Table 3, the OPA oscillator strengths for states 5, 6, and 7 (for CAM-B3LYP in the gas phase) are very small compared to the large TPA cross sections. Values for contributing dipole moment elements are shown in Table 5. The contributing transition

Table 5. Non-zero Dipole-Moment Elements Contributing to the TPA cross-section of the 5th, 6th, and 7th Excited States of the RFP Chromophore Determined at the CAM-B3LYP/6-31+G(d,p) Level of Theory in the Gas Phase

dipole element	value (Debye)
$ \langle 0 \mu 5 \rangle ^2$	1.07
$ \langle 0 \mu 1 \rangle ^2$	19.79
$ \langle 1 \mu 5 \rangle ^2$	0.13
$ \langle 5 \mu 5 \rangle - \langle 0 \mu 0 \rangle ^2$	0.44
$ \langle 0 \mu 6 \rangle ^2$	2.48
$ \langle 1 \mu 6 \rangle ^2$	0.29
$ \langle 6 \mu 6 \rangle - \langle 0 \mu 0 \rangle ^2$	0.44
$ \langle 0 \mu 7 \rangle ^2$	0.10
$ \langle 1 \mu 7 \rangle ^2$	0.03
$ \langle 7 \mu 7 \rangle - \langle 0 \mu 0 \rangle ^2$	3.64

dipole moments and the difference between permanent dipole moments of excited and ground states are collectively too weak to drive this strong absorption. For the CAM-B3LYP computations in the gas phase, energies of the involved transitions are comparable to twice of the first excited state energy of 2.477 eV. This causes the denominator of eq 2 to be small causing the amplification of these cross sections. These near-resonance conditions can be considered a key contributor to the large cross sections obtained confirming what has been shown before.^{16,18}

BFP. The values shown in Table 4 are for the BFP₁ model. The second excited state in all computations was dim, so there is no intermediate peak between the S₁ and the significant S_n peak, which is similar to the experimental spectra. The largest TPA cross-section belongs to the third excited state for all functionals. The computed energies using B3LYP and PBE0 (4.42 and 4.54 eV, respectively) match very well with the average experimental energy of 4.50 eV. On the other hand, CAM-B3LYP and LC-BLYP overestimate the energy. The cross sections determined for all functionals, however, are too large compared to the experimental average. The experimental spectra of all the involved proteins show a very sharp rise at approximately 4.5 eV, but each spectrum is discontinued before showing the descending part of the curve. The sharp slope indicates that the energy of the true spectroscopic peak is probably very close to the reported energy, but the TPA cross-section could be larger. The deviation of energies computed using CAM-B3LYP and LC-BLYP functionals from the experimental value is slightly larger in the S_n states than the behavior observed in the S₁ state.

CFP. The second lowest-energy transition with nonzero TPA in the case of CFP is given by the second state for B3LYP and PBE0 and the third state for CAM-B3LYP and LC-BLYP as shown in Table S15 in the Supporting Information. The state is relatively dim in the case of B3LYP and PBE0 (9 GM and 8 GM, respectively), weakly bright for CAM-B3LYP (23 GM) and very bright in case of LC-BLYP (123 GM). These transitions have a small value for the Λ diagnostic (0.42 for both B3LYP and PBE0, 0.46 for CAM-B3LYP, and 0.55 for LC-BLYP), characterizing a long-range excitation. The fourth transition computed using all functionals is shown in Table 4. Unlike the preceding transition, the fourth state is a valence-type excitation and is strongly bright as computed by all the functionals, so it is considered the main S_n transition. Experimentally, the spectra for ECFP and mCerulean⁷⁴ exhibit a smaller peak at an average energy of 3.78 eV with a TPA cross-section of 13 GM. This matches the computed long-range excitation state where B3LYP and PBE0 compute the energies to be 3.71 and 3.89 eV and the cross sections to be 9 GM and 8 GM, respectively. The experimental spectra show a sharp rise at 4.509 eV for both proteins with the average cross-section of 21 GM as in Table 4. As the spectrum ended abruptly at this energy, the experimentally reported cross-section could be underestimated. Our computed values estimate a larger cross-section than the largest determined value. When energies are compared, we notice a large variation between functionals (approximately 0.9 eV). The deviation from the experimental energy follows a trend similar to that seen with the BLB chromophore and to a lesser extent OR_A where the energy is lower for B3LYP and PBE0 and higher for CAM-B3LYP and LC-BLYP compared to the experimental one.

GFP. For GFP_A, as in CFP and RFP_A, there is a lower-energy state for each functional (see Table S15 in the Supporting Information) with a weak TPA cross-section ranging from 8 GM for B3LYP to 14 GM for LC-BLYP. This resembles the experimental spectra of some proteins that have the GFP chromophore such as mWasabi.⁷⁵ The experimental average for such a peak is 3.73 eV with a cross-section of 11 GM. Using B3LYP and PBE0, this band is computed to be at 4.19 and 4.32 eV and of cross-section 8 GM and 6 GM, respectively. On the other hand, the energy and cross-section for the higher-energy peak match very well with the experimental average (4.30 eV, 13 GM) with B3LYP (4.23 eV, 15 GM) and PBE0 (4.36 eV, 24

GM) performing better than CAM-B3LYP (4.76 eV, 95 GM) and LC-BLYP (4.90 eV, 188 GM). It is important to mention that the quoted experimental average of the highest energy peak is also for the highest value measured in that region and not for a true peak, but the rising curve is not steep indicating that the peak is most probably not much higher than the reported value. The analysis for GFP_N is very similar to that of GFP_A, as can be seen from Table 4 and Supporting Information, Table S16, and from the experimental TPA curves of proteins containing the GFP_N chromophore (mAmetrine,³⁵ for example).

KO_A. The experimental spectrum for mKok does not show an intermediate peak between the S₁ absorption and the sharp rise in the higher energy range. It only shows a shoulder peak at 3.4 eV. All functionals predict 4 higher groups of excitations following the transition to S₁ with large TPA cross sections (see Supporting Information, Table S16). Table 4 shows the second group, which corresponds to the fourth transition for B3LYP and PBE0 (3.62 and 3.77 eV). This group is preceded according to B3LYP and PBE0 by a very close peak, which is the third transition, at 3.51 and 3.69 eV, respectively. This lower energy peak might be interpreted as the shoulder peak in the experimental spectra. Both the energy of the fourth state and its cross-section for B3LYP and PBE0 (77 GM and 107 GM, respectively) match the experimental results nicely (3.62 eV and 93 GM) but are largely exaggerated by CAM-B3LYP (4.17 eV and 820 GM) and LC-BLYP (4.31 eV and 1355 GM). Further computed higher-energy excitations could not be correlated to the experimental spectrum, as it is attenuated at 3.62 eV.

OR_A. As with KO_A, four groups of higher excitations with large TPA cross sections were computed in the case of OR_A. Table 4 shows the first group which corresponds to the third excited state. The experimental data refers to the highest measured value in the high energy range of mOrange, but the rising curve starts to bend before it is attenuated suggesting that the measured value is very close to the true peak. As in the previous cases, excitation energies and TPA cross sections for B3LYP (3.65 eV and 87 GM) and PBE0 (3.80 eV and 121 GM) are closer to the experimental values (3.88 eV and 200 GM) than for CAM-B3LYP (4.21 eV and 754 GM) and LC-BLYP (4.35 eV and 1281 GM). Again, computed higher-energy excitations could not be correlated to the experimental spectrum, as it ended at the aforementioned energy point (3.88 eV).

BLB. The four functionals predict a lower-energy excitation before the one reported in Table 4, with very weak nonzero TPA cross-section (3 GM according to B3LYP and PBE0). At this lower energy, the experimental curve starts to rise to form the stronger TPA peak. The experimental curve is attenuated at 4.51 eV at a cross section of 22 GM. For both S₁ and S_n excitations, there is significant variation between experimental and computed cross sections for mBlueberry1. Excitation energies, OPA oscillator strengths, and TPA cross sections for the model having the acylimine moiety out-of-plane can be found in Supporting Information, Table S16. The crystal structure of a similar protein, Rtms5⁷⁶ (PDB ID: 3VK1), shows that the rings of the BLB chromophore are noncoplanar and assume a trans conformer (c.f. the cis conformer presented here). Computing TPA for the conformer where the experimental geometry is taken from the experimental X-ray structure (with hydrogen capping at the B3LYP/6-31+G(d,p) level of theory in PCM) resulted in a cross-section of approximately zero GM (data not shown). This observation

supports the hypothesis that the weak TPA that is experimentally observed for mBlueberry1 might be due to the distorted conformation its chromophore adopts. Unfortunately, there is no crystal structure for mBlueberry1, so we cannot decisively explore the deviation between experimental and computed cross sections.

4. CONCLUSIONS

TDDFT was used on isolated chromophores to evaluate the efficiency of PBE0, B3LYP, CAM-B3LYP, and LC-BLYP functionals in reproducing TPA absorption energies and cross sections of the corresponding FPs both in the gas phase and in water (PCM). Gas-phase computations yield larger TPA cross sections than the corresponding ones in water. Energies and cross sections of the first transition (lowest energy) are less functional dependent than the higher-energy transitions. For this first transition, the TPA energies and cross sections computed by CAM-B3LYP and LC-BLYP are systematically larger than the corresponding B3LYP and PBE0 values. We compared the computed vertical excitation energies to the TPA experimental energies (that are blue-shifted for many systems due to the involved vibronic transition) and to CC2 energies. The experimental lowest-energy was generally lower than the computed vertical excitation energy for the first transition and thus best reproduced with B3LYP (which generally gave the lowest energies). The TDDFT energies were, in general, lower than the corresponding CC2 ones. Within the present approximations neglecting vibronic and environmental effects, the experimental TPA cross sections are not quantitatively reproduced by any of the functionals which renders TDDFT good at only qualitative or semiquantitative analysis. The situation is worse when it comes to higher-energy transitions. This is not very surprising provided the substantial variability in the experimental TPA cross sections of various proteins sharing the same chromophore. This is a proposed limitation as long as the study involves the isolated chromophores and ignores the protein shell. The electric field of the protein and conformational restraints exerted by the surrounding residues can significantly alter the TPA of the chromophore. The conformational dependence was highlighted here in the discussion of the RFP (BLB) chromophore where the carbonyl rotation considerably increased (decreased) the TPA cross-section. Therefore, when screening chromophores with conformational flexibility for TPA, one should consider carefully the role of the conformation on the TPA cross-section. For the higher-energy transitions, CAM-B3LYP and LC-BLYP predictions for both TPA cross sections and energies deviated significantly from the experimental values discouraging their use in any future TPA analysis. The erroneous overestimation of cross sections is caused by the artificial resonance enhancement of the TPA for the S_n state. On the other hand, B3LYP (and PBE0) yielded energies and TPA cross sections that are close to the averaged experimental values. The use of B3LYP (and PBE0) is suitable for computational screening of TPA to S_n . This conclusion is based on the present formalism adopting undamped response theory. Including a damping coefficient might change the behavior of the functionals, but this is not discussed in the present study. Moreover, care must be taken if one considers a more detailed analysis of the excited states as in some cases (e.g., RFP_A and KO_A, see Tables 3 and 4), the energetic ordering may be incorrect for B3LYP and PBE0 due to the presence of low-lying states with long-range (charge-transfer) excitation character. Overall for TDDFT studies on isolated FP

chromophores, we recommend, based on both energetics and absolute TPA cross sections, the use of B3LYP or PBE0 for the qualitative assessment of potential TPA probes accessing the lowest energy S_1 states.

■ ASSOCIATED CONTENT

Supporting Information

Data for the various computations done at the TDDFT/6-31+G(d,p) level of theory in the gas phase and PCM (water), plots of orbitals involved in the studied excited-states of all the included systems, the grouping of bright excitations based on visual inspection of these orbitals, experimental data, and coordinates of the optimized systems. This material is available free of charge via the Internet at <http://pubs.acs.org/>.

■ AUTHOR INFORMATION

Corresponding Author

*Email: alex.brown@ualberta.ca.

Notes

The authors declare no competing financial interest.

■ ACKNOWLEDGMENTS

We thank Dr. M. Drobizhev and Dr. R. Nifosi for fruitful discussions. We also thank Prof. Peter R. Taylor and Dr. Alfredo J. Sánchez de Merás for support with the DALTON program. We thank the Natural Sciences and Engineering Research Council (NSERC) of Canada for financial support and the Canadian Foundation for Innovation (New Opportunities Fund) for support for computational infrastructure. This research has been (partially) enabled by the use of computing resources provided by WestGrid and Compute/Calcul Canada.

■ REFERENCES

- (1) Shimomura, O.; Johnson, F. H.; Saiga, Y. *J. Cell. Comp. Physiol.* **1962**, *59*, 223–229.
- (2) Prasher, D. C.; Eckenrode, V. K.; Ward, W. W.; Prendergast, F. G.; Cormier, M. J. *Gene* **1992**, *111*, 229–233.
- (3) Chalfie, M.; Tu, Y.; Euskirchen, G.; Ward, W. W.; Prasher, D. *Science* **1994**, *263*, 802–805.
- (4) Inouye, S.; Tsuji, F. I. *FEBS Lett.* **1994**, *341*, 277–280.
- (5) Nifosi, R.; Tozzini, V. One-Photon and Two-Photon Excitation of Fluorescent Proteins. In *Fluorescent Proteins I*; Jung, G., Ed.; Springer: Berlin Heidelberg, 2012; Vol. 11, pp 3–40.
- (6) Shaner, N. C.; Steinbach, P. A.; Tsien, R. Y. *Nat. Methods* **2005**, *2*, 905–909.
- (7) Ormo, M.; Cubitt, A. B.; Kallio, K.; Gross, L. A.; Tsien, R. Y.; Remington, S. *Science* **1996**, *273*, 1392–1395.
- (8) Yang, F.; Moss, L. G.; Phillips, G. *Nat. Biotechnol.* **1996**, *14*, 1246–1251.
- (9) Wachter, R. M.; Elsliger, M. A.; Kallio, K.; Hanson, G. T.; Remington, S. J. *Structure* **1998**, *6*, 1267–1277.
- (10) Drobizhev, M.; Tillo, S.; Makarov, N. S.; Hughes, T. E.; Rebane, A. *J. Phys. Chem. B* **2009**, *113*, 855–859.
- (11) Blab, G. A.; Lommerse, P. H.; Cognet, L.; Harms, G. S.; Schmidt, T. *Chem. Phys. Lett.* **2001**, *350*, 71–77.
- (12) Ai, Y.; Tian, G.; Luo, Y. *Mol. Phys.* **2013**, *111*, 1316–1321.
- (13) Kamarchik, E.; Krylov, A. I. *J. Phys. Chem. Lett.* **2011**, *2*, 488–492.
- (14) Drobizhev, M.; Makarov, N. S.; Tillo, S. E.; Hughes, T. E.; Rebane, A. *J. Phys. Chem. B* **2012**, *116*, 1736–1744.
- (15) List, N. H.; Olsen, J. M. H.; Jensen, H. J. A.; Steindal, A. H.; Kongsted, J. *J. Phys. Chem. Lett.* **2012**, *3*, 3513–3521.
- (16) Nifosi, R.; Luo, Y. *J. Phys. Chem. B* **2007**, *111*, 14043–14050.

- (17) Drobizhev, M.; Makarov, N. S.; Tillo, S. E.; Hughes, T. E.; Rebane, A. *Nat. Methods* **2011**, *8*, 393–399.
- (18) Drobizhev, M.; Makarov, N. S.; Hughes, T.; Rebane, A. *J. Phys. Chem. B* **2007**, *111*, 14051–14054.
- (19) Marchant, J. S.; Stutzmann, G. E.; Leissring, M. A.; LaFerla, F. M.; Parker, I. *Nat. Biotechnol.* **2001**, *19*, 645–649.
- (20) Tillo, S. E.; Hughes, T. E.; Makarov, N. S.; Rebane, A.; Drobizhev, M. *BMC Biotechnol.* **2010**, *10*, 6.
- (21) Steindal, A. H.; Olsen, J. M. H.; Ruud, K.; Frediani, L.; Kongsted, J. *Phys. Chem. Chem. Phys.* **2012**, *14*, 5440–5451.
- (22) Paterson, M. J.; Christiansen, O.; Pawlowski, F.; Jørgensen, P.; Hättig, C.; Helgaker, T.; Salek, P. *J. Chem. Phys.* **2006**, *124*, 054322.
- (23) Nayyar, I. H.; Tretiak, S. *J. Phys. Chem. C* **2013**, *117*, 18170–18189.
- (24) Day, P. N.; Nguyen, K. A.; Pachter, R. *J. Phys. Chem. B* **2005**, *109*, 1803–1814.
- (25) Beerepoot, M. T. P.; Friese, D. H.; Ruud, K. *Phys. Chem. Chem. Phys.* **2014**, *16*, 5958–5964.
- (26) Friese, D. H.; Hättig, C.; Ruud, K. *Phys. Chem. Chem. Phys.* **2012**, *14*, 1175–1184.
- (27) Matz, M. V.; Fradkov, A. F.; Labas, Y. A.; Savitsky, A. P.; Zarausky, A. G.; Markelov, M. L.; Lukyanov, S. A. *Nat. Biotechnol.* **1999**, *17*, 969–973.
- (28) Gross, L. A.; Baird, G. S.; Hoffman, R. C.; Baldrige, K. K.; Tsien, R. Y. *Proc. Natl. Acad. Sci. U.S.A.* **2000**, *97*, 11990–11995.
- (29) Wachter, R. M.; Watkins, J. L.; Kim, H. *Biochemistry* **2010**, *49*, 7417–7427.
- (30) Ai, H.-W.; Shaner, N. C.; Cheng, Z.; Tsien, R. Y.; Campbell, R. E. *Biochemistry* **2007**, *46*, 5904–5910.
- (31) Wachter, R. M.; King, B. A.; Heim, R.; Kallio, K.; Tsien, R. Y.; Boxer, S. G.; Remington, S. J. *Biochemistry* **1997**, *36*, 9759–9765.
- (32) Heim, R.; Prasher, D. C.; Tsien, R. Y. *Proc. Natl. Acad. Sci. U.S.A.* **1994**, *91*, 12501–12504.
- (33) Chattoraj, M.; King, B. A.; Bublit, G. U.; Boxer, S. G. *Proc. Natl. Acad. Sci. U.S.A.* **1996**, *93*, 8362–8367.
- (34) Kikuchi, A.; Fukumura, E.; Karasawa, S.; Mizuno, H.; Miyawaki, A.; Shiro, Y. *Biochemistry* **2008**, *47*, 11573–11580.
- (35) Shaner, N. C.; Campbell, R. E.; Steinbach, P. A.; Giepmans, B. N. G.; Palmer, A. E.; Tsien, R. Y. *Nat. Biotechnol.* **2004**, *22*, 1567–1572.
- (36) Shu, X.; Shaner, N. C.; Yarbrough, C. A.; Tsien, R. Y.; Remington, S. J. *Biochemistry* **2006**, *45*, 9639–9647.
- (37) (a) Perdew, J. P.; Burke, K.; Ernzerhoff, M. *Phys. Rev. Lett.* **1996**, *77*, 3865–3868. (b) Perdew, J. P.; Burke, K.; Ernzerhoff, M. *Phys. Rev. Lett.* **1996**, *78*, 1396.
- (38) Adamo, C.; Barone, V. *J. Chem. Phys.* **1999**, *110*, 6158–6169.
- (39) Ditchfield, R.; Hehre, W. J.; Pople, J. A. *J. Chem. Phys.* **1971**, *54*, 724–728.
- (40) Hehre, W. J.; Ditchfield, R.; Pople, J. A. *J. Chem. Phys.* **1972**, *56*, 2257–2261.
- (41) Francl, M. M.; Pietro, W. J.; Hehre, W. J.; Binkley, J. S.; Gordon, M. S.; DeFrees, D. J.; Pople, J. A. *J. Chem. Phys.* **1982**, *77*, 3654–3665.
- (42) Hariharan, P.; Pople, J. *Theor. Chim. Acta* **1973**, *28*, 213–222.
- (43) Clark, T.; Chandrasekhar, J.; Spitznagel, G. W.; Schleyer, P. V. *R. J. Comput. Chem.* **1983**, *4*, 294–301.
- (44) Runge, E.; Gross, E. K. U. *Phys. Rev. Lett.* **1984**, *52*, 997–1000.
- (45) Casida, M. E. Time-dependent density functional theory for molecules. In *Recent Advances in Density Functional Methods, Part I*; Chong, D. P., Ed.; World Scientific: Singapore, 1995; Chapter 5, pp 155–192.
- (46) Salek, P.; Vahtras, O.; Guo, J.; Luo, Y.; Helgaker, T.; Agren, H. *Chem. Phys. Lett.* **2003**, *374*, 446–452.
- (47) Frediani, L.; Rinkevicius, Z.; Agren, H. *J. Chem. Phys.* **2005**, *122*, 244104.
- (48) Tretiak, S.; Chernyak, V. *J. Chem. Phys.* **2003**, *119*, 8809–8823.
- (49) Becke, A. D. *J. Chem. Phys.* **1993**, *98*, 5648–5652.
- (50) Yanai, T.; Tew, D. P.; Handy, N. C. *Chem. Phys. Lett.* **2004**, *393*, 51–57.
- (51) Iikura, H.; Tsuneda, T.; Yanai, T.; Hirao, K. *J. Chem. Phys.* **2001**, *115*, 3540–3544.
- (52) Lee, C.; Yang, W.; Parr, R. G. *Phys. Rev. B* **1988**, *37*, 785–789.
- (53) Becke, A. D. *Phys. Rev. A* **1988**, *38*, 3098–3100.
- (54) Tawada, Y.; Tsuneda, T.; Yanagisawa, S.; Yanai, T.; Hirao, K. *J. Chem. Phys.* **2004**, *120*, 8425–8433.
- (55) Barone, V.; Cossi, M. *J. Phys. Chem. A* **1998**, *102*, 1995–2001.
- (56) Cossi, M.; Rega, N.; Scalmani, G.; Barone, V. *J. Comput. Chem.* **2003**, *24*, 669–681.
- (57) Tomasi, J.; Mennucci, B.; Cammi, R. *Chem. Rev.* **2005**, *105*, 2999–3094.
- (58) Cossi, M.; Barone, V. *J. Chem. Phys.* **2001**, *115*, 4708–4717.
- (59) Christiansen, O.; Koch, H.; Jørgensen, P. *Chem. Phys. Lett.* **1995**, *243*, 409–418.
- (60) Hättig, C.; Christiansen, O.; Jørgensen, P. *J. Chem. Phys.* **1998**, *108*, 8331–8354.
- (61) Cronstrand, P.; Luo, Y.; Agren, H. *Adv. Quantum Chem.* **2005**, *50*, 1.
- (62) Peach, M. J. G.; Benfield, P.; Helgaker, T.; Tozer, D. J. *J. Chem. Phys.* **2008**, *128*, 044118.
- (63) DALTON2013, a molecular electronic structure program, 2013. Available online: <http://www.daltonprogram.org>.
- (64) Schmidt, M. W.; Baldridge, K. K.; Boatz, J. A.; Elbert, S. T.; Gordon, M. S.; Jensen, J. H.; Koseki, S.; Matsunaga, N.; Nguyen, K. A.; Su, S. J.; Windus, T. L.; Dupuis, M.; Montgomery, J. A. *J. Comput. Chem.* **1993**, *14*, 1347–1363.
- (65) Bode, B. M.; Gordon, M. S. *J. Mol. Graphics Model.* **1998**, *16*, 133–138.
- (66) Zhang, G.; Gurtu, V.; Kain, S. R. *Biochem. Biophys. Res. Commun.* **1996**, *227*, 707–711.
- (67) Hosoi, H.; Yamaguchi, S.; Mizuno, H.; Miyawaki, A.; Tahara, T. *J. Phys. Chem. B* **2008**, *112*, 2761–2763.
- (68) Kawano, H.; Kogure, T.; Abe, Y.; Mizuno, H.; Miyawaki, A. *Nat. Methods* **2008**, *5*, 373–374.
- (69) Subach, O. M.; Gundorov, I. S.; Yoshimura, M.; Subach, F. V.; Zhang, J.; Grünwald, D.; Souslova, E. a.; Chudakov, D. M.; Verkhusha, V. V. *Chem. Biol.* **2008**, *15*, 1116–1124.
- (70) Timerghazin, Q. K.; Carlson, H. J.; Liang, C.; Campbell, R. E.; Brown, A. *J. Phys. Chem. B* **2008**, *112*, 2533–2541.
- (71) Xu, Y. W.; Zhang, J. R.; Deng, Y. M.; Hui, L. K.; Jiang, S. P.; Lian, S. H. *J. Photochem. Photobiol., B* **1987**, *1*, 223–227.
- (72) Sengupta, P.; Balaji, J.; Mukherjee, S.; Philip, R.; Ravindra Kumar, G.; Maiti, S. *Proc. SPIE-Int. Soc. Opt. Eng.* **2001**, *4262*, 336–339.
- (73) Merzlyak, E. M.; Goedhart, J.; Shcherbo, D.; Bulina, M. E.; Shcheglov, A. S.; Fradkov, A. F.; Gaintzeva, A.; Lukyanov, K. A.; Lukyanov, S.; Gadella, T. W. J.; Chudakov, D. M. *Nat. Biotechnol.* **2007**, *4*, 555–557.
- (74) Rizzo, M. A.; Springer, G. H.; Granada, B.; Piston, D. W. *Nat. Biotechnol.* **2004**, *22*, 445–449.
- (75) Ai, H.-W.; Olenych, S. G.; Wong, P.; Davidson, M. W.; Campbell, R. E. *BMC Biol.* **2008**, *6*, 13.
- (76) Battad, J. M.; Traore, D. A. K.; Byres, E.; Rossjohn, J.; Devenish, R. J.; Olsen, S.; Wilce, M. C. J.; Prescott, M. *PLoS One* **2012**, *7*, e47331.